Chemical Science

RSC Publishing

EDGE ARTICLE

View Article Online
View Journal | View Issue

Enhanced isosteric heat, selectivity, and uptake capacity of CO_2 adsorption in a metal-organic framework by impregnated metal ions†

Cite this: *Chem. Sci.*, 2013, **4**, 685

Hye Jeong Park and Myunghyun Paik Suh*

We demonstrate by experimental and theoretical studies that the impregnation of various metal ions such as Li^+, Mg^{2+}, Ca^{2+}, Co^{2+}, and Ni^{2+} in the pores of an anionic MOF, $[Zn_3(TCPT)_2(HCOO)][NH_2(CH_3)_2]$ (**SNU-100′**) significantly enhances isosteric heat, selectivity, and uptake capacity of the CO_2 adsorption in the MOF. Due to the electrostatic interactions between CO_2 and the extra-framework metal ions, the isosteric heats of CO_2 adsorption are increased to 37.4–34.5 kJ mol^{-1} and the adsorption selectivities of CO_2 over N_2 at room temperature are increased to 40.4–31.0, compared with those (29.3 kJ mol^{-1} and 25.5, respectively) of the parent MOF (**SNU-100′**) containing $[NH_2(CH_3)_2]^+$ cations.

Received 14th August 2012
Accepted 30th October 2012

DOI: 10.1039/c2sc21253f

www.rsc.org/chemicalscience

Introduction

Porous metal-organic frameworks (MOFs) have attracted significant interest due to their potential to be applied in hydrogen storage,[1] carbon dioxide capture,[2] and O_2/N_2 gas separation.[3] In particular, selective and reversible capture of carbon dioxide from industrial flue gas has become one of the most important issues recently in the scientific community. Industrial flue gas contains not only carbon dioxide but also other gases, and its composition is dependent on the combustion methods. The flue gas emitted from the post-combustion chamber has a pressure of 1 atm with 15% of CO_2, 75% of N_2, 5–10% of water vapour, and other minor components such as O_2, SO_x, NO_x, and CO. To apply a MOF in capturing CO_2 from industrial flue gas that is emitted from a post-combustion chamber, its storage capacity at ambient temperatures under low pressure (0.15 atm) of CO_2 and adsorption selectivity for CO_2 over other gases should be high. For practical applications, the stability of the framework against water vapour as well as the effects of water vapour and other minor components of the flue gas on the separation of CO_2 must be also considered.

MOFs which have high surface area and pore volume show high CO_2 adsorption capacity at room temperature under high pressures.[4] For example, MOF-177 that has a BET surface area of 4500 m^2 g^{-1} can store 60.8 wt% (750 cm^3 g^{-1}) of CO_2 at 298 K and 35 bar.[4d] However, under 1 atm and at 298 K, the CO_2 storage capacity of MOF-177 decreases to 3.4 wt%. In addition, the selectivity for CO_2 adsorption over N_2 in MOF-177 calculated by using the molar ratio of the CO_2 uptake at 0.15 atm and the N_2 uptake at 0.85 atm is only 4.[2a] The isosteric heat (Q_{st}) of CO_2 adsorption in common MOFs ranges from 25–35 kJ mol^{-1}.[2a] It was reported that Cu-BTTri-en[5] and Cu-BTTri-mmen[6] whose metal sites were functionalized with ethylenediamine and *N,N′*-dimethylethylenediamine, respectively, exhibited zero-coverage Q_{st} values of 90 and 96 kJ mol^{-1}, respectively, which were too high to reversibly release CO_2 from the amine moieties without applying heat. To increase the CO_2 adsorption capacity together with the adsorption selectivity for CO_2 over other gases at ambient temperature under the CO_2 pressure of *ca.* 0.15 atm, the Q_{st} value of CO_2 adsorption should be increased to a certain extent that minimizes the energy penalty for regeneration.

Here we report for the first time based on experimental and theoretical studies that the impregnation of various metal ions such as Li^+, Mg^{2+}, Ca^{2+}, Co^{2+}, and Ni^{2+} in the pores of an anionic MOF significantly increases the Q_{st} value of CO_2 adsorption in the MOF to the range of 37.4–34.5 kJ mol^{-1} as well as the adsorption selectivity of CO_2 over N_2 to 40.4–31.0, and thus enhances the CO_2 capture ability at room temperature.

Results and discussion

We have prepared a new anionic MOF including dimethylammonium cations in the 1D channels, $[Zn_3(TCPT)_2(HCOO)][NH_2(CH_3)_2]\cdot 5DMF$ (**SNU-100**, TCPT = 2,4,6-tris-(4-carboxyphenoxy)-1,3,5-triazine), by heating the DMF solution of $Zn(NO_3)_2\cdot 6H_2O$ and H_3TCPT at 90 °C for 24 h. In the X-ray structure of **SNU-100**, there exist crystallographically independent two Zn(II) centers (Zn1 and Zn2) and they are linked in the sequence of Zn1–Zn2–Zn1 to form a Zn_3 cluster unit (Fig. S1†).

Department of Chemistry, Seoul National University, Seoul 151-747, Republic of Korea. E-mail: mpsuh@snu.ac.kr; Fax: +82-2-886-8516; Tel: +82-2-880-7760

† Electronic supplementary information (ESI) available: Detailed experimental procedures, ORTEP drawings, TGA/DSC traces, PXRD patterns, temperature dependent PXRD patterns, additional gas sorption isotherms, fitting curves for calculation of isosteric heats and selectivities for various gases, tables of X-ray data for **1**, tables of fitting parameters, and tables of gas adsorption data. CCDC 869629. For ESI and crystallographic data in CIF or other electronic format see DOI: 10.1039/c2sc21253f

Zn1 and Zn2 show a tetrahedral- [∠O–Zn–O, av. 116.88(3)°] and an octahedral-coordination geometry, respectively. Three Zn_3 cluster units are connected by two $TCPT^{3-}$ linkers infinitely to form 2D layers, which run parallel to the *ab* plane (Fig. S2†). The triazine rings of the two $TCPT^{3-}$ are nearly coplanar and form a 'D_3-Piedfort unit'.[7] The 2D layers are linked by formate species along the *c* axis, which gives rise to a 3D anionic framework. In **SNU-100**, two 3D frameworks are mutually interpenetrated to generate 1D channels where dimethylammonium cations are included (Fig. 1). The solvent accessible volumes of **SNU-100** with and without dimethylammonium are 14.5 and 38.1%, respectively, as estimated by PLATON.[8] The guest solvent molecules included in the pores could not be refined, and they were characterized by the IR, elemental analysis (EA), and thermogravimetric analysis (TGA) data (Fig. S3†).

When the single crystals of **SNU-100** were immersed in MeOH for 2 days, the guest solvent molecules were exchanged to provide $[Zn_3(TCPT)_2(HCOO)][NH_2(CH_3)_2]\cdot 6MeOH$ (**SNU-100m**). When **SNU-100m** was activated at 60 °C under vacuum for 2 h, the desolvated solid $[Zn_3(TCPT)_2(HCOO)][NH_2(CH_3)_2]$ (**SNU-100′**) was resulted. The powder X-ray diffraction (PXRD) patterns of **SNU-100m** and **SNU-100′** were coincident with that of **SNU-100**, indicating that the framework structure could be retained during the guest–solvent exchange and guest-removal processes (Fig. S8†). Interestingly, the framework structure of **SNU-100′** was retained even after the exposure to water vapor for 7 days or immersion in water for 7 days, as evidenced by the PXRD patterns (Fig. S9†). The stability of the framework that contains tetrahedral Zn^{2+} ions against water may be attributed to the interpenetrated nature and/or the anionic charge of the framework, in addition to the coordinated formate that links secondary building units.[7] To explain this better, we will further conduct simulation works.

To verify the porosity of **SNU-100′**, sorption isotherms were measured for N_2, O_2, H_2, CO_2, and CH_4 gases (Table S2†). The N_2 sorption isotherm measured at 77 K showed typical Type-I sorption behaviour, characteristic for the microporosity (Fig. S10†). The BET surface area and the pore volume estimated by applying the Dubinin–Radushkevich (DR) equation are 814 $m^2\ g^{-1}$ and 0.315 $cm^3\ g^{-1}$, respectively. **SNU-100′** adsorbs H_2 gas up to 1.81 wt% at 77 K and 1 atm, and 1.30 wt% at 87 K and 1 atm (Fig. S11 and S12†). The Q_{st} values of H_2 adsorption in **SNU-100′** are 8.17–7.11 kJ mol^{-1} depending on the degree of H_2 loading (Fig. S13†), as estimated by fitting the H_2 isotherms at 77 K and 87 K to the virial equation (Fig. S14†).[9] The zero-coverage Q_{st} (8.17 kJ mol^{-1}) is significantly higher than those of the common MOFs such as MOF-5 (4.8 kJ mol^{-1}),[4d] because of the small pore size resulting from the interpenetration as well as the dimethylammonium cations included in the channels. The CO_2 gas adsorption isotherms of **SNU-100′** indicate that the material stores a large amount of CO_2, up to 3.20 mmol g^{-1} (71.6 $cm^3\ g^{-1}$ at STP, 14.1 wt%) at 298 K and 1 atm (Fig. 2a). After **SNU-100′** was exposed to water vapor for 7 days or immersed in water for 7 days, or after water vapor sorption was measured at 293 K (Fig. S15†), the CO_2 uptake capacity of **SNU-100′** was still maintained once the sample was reactivated at 60 °C under vacuum for 12 h (Fig. S16†). The Q_{st} of CO_2 adsorption in **SNU-100′** is 29.3–27.7 kJ mol^{-1} (Fig. 2b), as calculated by the Clausius–Clapeyron equation using dual-site Langmuir parameters at 231, 273, and 298 K (Fig. S20 and Table S8†). The selectivity for CO_2 adsorption over N_2 is 25.5, as estimated from the ratios of Henry constants obtained by the

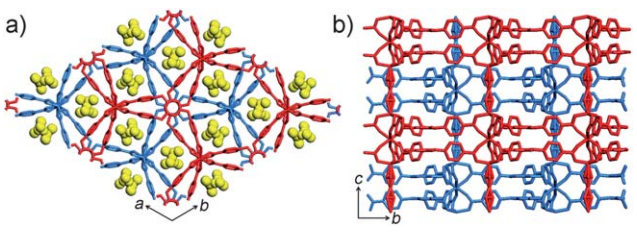

Fig. 1 X-Ray crystal structure of **SNU-100**. (a) View seen on the *ab* plane. (b) View seen on the *bc* plane. Doubly interpenetrated anionic frameworks are represented in two different colors (red and blue) and $[NH_2(CH_3)_2]^+$ cations refined are represented in yellow.

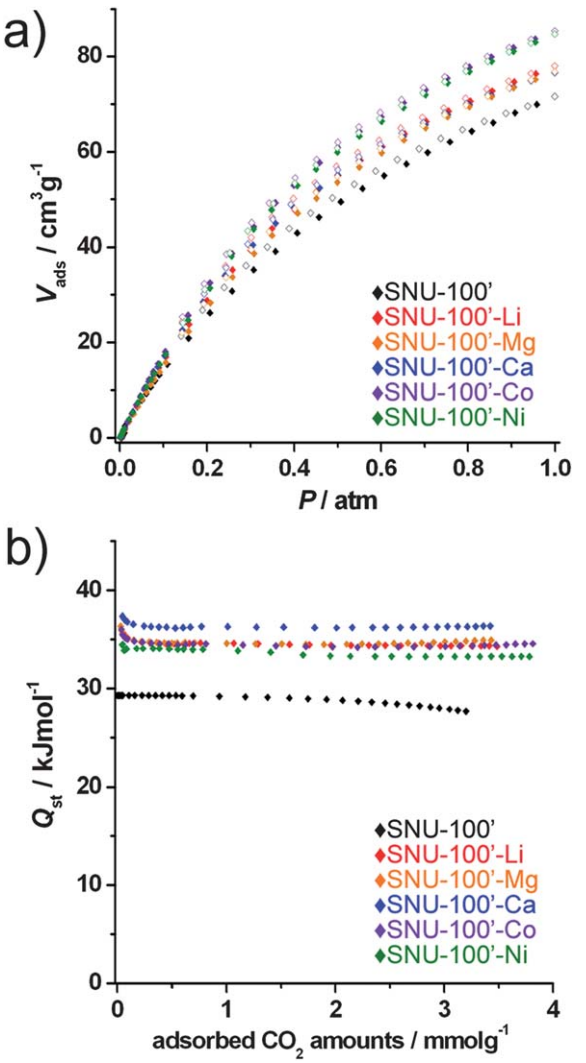

Fig. 2 (a) CO_2 sorption isotherms of **SNU-100′-M** at 298 K. Filled shapes: adsorption. Open shapes: desorption. (b) Q_{st} of CO_2 adsorption.

Langmuir equation (Fig. S21†). These values are comparable to those of ZIF-79[10] and higher than BPL carbon that is widely used in the industry for gas separations.[11]

To investigate the effect of the impregnated metal ions in the pores of the MOF on the gas sorption properties, the dimethylammonium included in **SNU-100m** was post-synthetically exchanged with Li^+, Mg^{2+}, Ca^{2+}, Co^{2+}, and Ni^{2+} ions, which afforded **SNU-100-Li**, **SNU-100-Mg**, **SNU-100-Ca**, **SNU-100-Co**, and **SNU-100-Ni**, respectively. In the experiments, crystals of **SNU-100m** (*ca.* 0.10 mmol) were immersed in the MeOH solutions of various hydrated metal salts, such as $LiCl\cdot xH_2O$, $Mg(NO_3)_2\cdot 6H_2O$, $Ca(NO_3)_2\cdot 4H_2O$, $Co(NO_3)_2\cdot 6H_2O$, and $Ni(NO_3)_2\cdot 6H_2O$ (concentration, 0.0970–0.126 M) for 10 days. Some of the **SNU-100-M** samples maintained the single crystallinity, but they provided poor X-ray diffraction data. After drying **SNU-100-M** at 60 °C under vacuum for 12 h, the degree of metal ion impregnation was determined by Inductively Coupled Plasma-Atomic Emission Spectroscopy (ICP-AES). The ICP-AES data indicate that 84.4–95.4% of the dimethylammonium cations were exchanged with Li^+, Mg^{2+}, Ca^{2+}, Co^{2+}, and Ni^{2+}. Unexpectedly, however, with Fe^{2+} and Cu^{2+} ions, even the intra-framework Zn^{2+} ions as well as the extra-framework ammonium cations were substituted with the metal ions. The trivalent metal ions such as Al^{3+} and Fe^{3+} could not be included because the framework was dissociated in the MeOH solutions of the trivalent metal salts even when the concentrations were low (1.0 mM). The chemical formula of the frameworks impregnating various metal ions, **SNU-100′-M**, which were activated by heating at 60 °C under vacuum for 12 h, were determined based on the relative mass ratios of M/Zn, together with the elemental analysis data. The results suggested that the introduced metal ions still bound 4–6 water molecules. These water molecules are also evidenced by the IR spectra of **SNU-100′-M**, which show OH stretching and HOH bending modes at 3641–3647 cm^{-1} and 1629 cm^{-1}, respectively (Fig. S22†). These coordinated water molecules must be originated from the metal salts used in the cation exchange process. The PXRD patterns indicate that the series of **SNU-100′-M** have the same structure as that of **SNU-100′** (Fig. S8†). Even after exposure to water vapor for 7 days, the framework of **SNU-100′-M** remained stable as evidenced by PXRD patterns (Fig. S9†).

The N_2 sorption isotherms of **SNU-100′-M** measured at 77 K showed typical Type-I sorption behavior with no hysteresis upon desorption (Fig. S10†). The BET surface areas ranged from 924 $m^2\ g^{-1}$ for **SNU-100′-Li** to 1000 $m^2\ g^{-1}$ for **SNU-100′-Co**, slightly higher than that of **SNU-100′**. Since there are relatively few anionic MOFs that can retain their porosity after cation exchange,[12] the present results are significant.

The H_2 storage capacities at 77 K and 87 K under the pressure of up to 1 atm for the series of **SNU-100′-M** increased compared with that of **SNU-100′** (Table 1, Fig. S11 and S12†), which must be attributed to the increased accessible surface areas and pore volumes of **SNU-100′-M**. The zero-coverage Q_{st} values of H_2 adsorption, which were estimated from the H_2 sorption isotherms at 77 K and 87 K by using the virial equation (Fig. S23–S27†), ranged from 8.40–7.01 kJ mol^{-1} (Fig. S13†), indicating that the impregnated metal ions exert rather minor effects on the interaction energy between H_2 and the MOF. We assume that the coordinated aqua ligands prevent direct access of H_2 molecules to the metal site. If metal ions were bare without coordinated solvent molecules, zero-coverage Q_{st} values of the H_2 adsorption should be increased by *ca.* 4–5 kJ mol^{-1}.[1a,13a] To improve Q_{st} of the H_2 adsorption in MOFs, various strategies[1a] have been employed such as creation of accessible metal sites,[13] incorporation of polarizing organic functional groups,[14] impregnation of metal nanoparticles[15] or metal ions[12] in the pores, and the exchange of metals within the metal nodes.[16] The post-synthetic exchange of dimethylammonium or protonated piperazine included in the MOFs with other metal ions such as Li^+ or Mg^{2+} only slightly (0.2–1.1 kJ mol^{-1}) increased Q_{st} values of the H_2 adsorption due to the solvent molecules still bound to the extra-framework metal ions.[12a] Similarly to our findings, the exchange of the guest Mn^{2+} ions in $Mn_3[(Mn_4Cl)_3(BTT)_8(CH_3OH)_{10}]_2$ with Li^+, Cu^+, Fe^{2+}, Co^{2+}, Ni^{2+}, Cu^{2+}, Zn^{2+} resulted in a difference of only 2 kJ mol^{-1} between the weakest and the strongest zero-coverage Q_{st} values for the samples since the metal ions bound solvent molecules.[12b]

As for the CO_2 adsorption, **SNU-100′** shows the highest CO_2 capacity at 195 K (Fig. S17†) among the present samples. However, at higher temperatures, **SNU-100′-M** with larger BET surface area adsorbs a larger amount of CO_2 than **SNU-100′** (Table 1, Fig. 2a, Fig. S18 and 19†). At 298 K and 1 atm, **SNU-100′-Co** can store 16.8 wt% of CO_2, which is the next highest value to the best data in the MOF-74 series (27.5–17.6 wt%)[17] and HKUST-1 (19.8 wt%).[18] For better understanding, we calculated Q_{st} values of CO_2 adsorption for **SNU-100′-M** by using the Clausius–Clapeyron equation based on dual-site Langmuir parameters at 231, 273, and 298 K (Fig. S28–S32 and Table S8†). Contrary to Q_{st} of H_2 adsorption, the low coverage Q_{st} values of the CO_2 adsorption in the **SNU-100′-M** series are increased to 37.4–34.5 kJ mol^{-1}, compared with that (29.3 kJ mol^{-1}) of **SNU-100′** (Table 1, Fig. 2b). These high Q_{st} values must be primarily attributed to the electrostatic field provided by the extra-framework metal ions[19] as well as the strong interaction of CO_2 with the water molecules coordinated at the metal ions.[18] The low coverage Q_{st} values of CO_2 adsorption in **SNU-100′-M** are higher than those in common MOFs (25–35 kJ mol^{-1}), but lower than the MOF-74 series (Mg-MOF-74, 47 kJ mol^{-1}; Ni-MOF-74, 42 kJ mol^{-1})[17] and MIL-100 (62 kJ mol^{-1}),[20] which contains open metal sites, and Cu-BTTri that is amine-functionalized at the metal site (90 kJ mol^{-1}).[5] On cation exchange with Co^{2+}, colorless crystals of **SNU-100m** changed to pink to form **SNU-100-Co**, which turned to purple on activation at 60 °C under vacuum for 12 h (Fig. S33†), suggesting that the coordination number of Co^{2+} changed from 6 to 4 upon activation. To see the effect of coordinated water molecules on CO_2 uptake, we attempted to remove the coordinated water molecules at Co^{2+} from **SNU-100′-Co**. For this, the sample was activated at 60, 100, 150, 200, 250, 300, 350, and 400 °C, respectively, and the CO_2 gas sorption isotherms were measured at 298 K. When the sample was activated at the temperatures lower than 350 °C under vacuum, the CO_2 uptake capacities were nearly the same as that of the sample activated at 60 °C under vacuum (Fig. S34†). However, the sample activated at 400 °C under vacuum showed much

Table 1 Gas sorption properties of **SNU-100′** and **SNU-100′-M** and comparison of the CO_2 adsorption data with other MOFs

Compound	Formula[a]	M/Zn ratio	SA_{BET} ($m^2\ g^{-1}$)	H_2 uptake (wt%)[b]	Q_{st} of H_2 (kJ mol^{-1})	CO_2 uptake (wt%)[c]	Q_{st} of CO_2 (kJ mol^{-1})	Selectivity of CO_2/N_2[d]
SNU-100′	$[Zn_3(TCPT)_2(HCOO)][NH_2(CH_3)_2]$	—	814	1.81	8.14–7.08	14.1	29.3–27.7	25.5 (26.5)
SNU-100′-Li	$[Zn_3(TCPT)_2(HCOO)][Li(H_2O)_n]_{0.844}[NH_2(CH_3)_2]_{0.156}$	0.281	924	1.93	8.40–5.91	15.3	35.7–34.3	37.8 (31.9)
SNU-100′-Mg	$[Zn_3(TCPT)_2(HCOO)][Mg(H_2O)_n]_{0.442}[NH_2(CH_3)_2]_{0.116}$	0.147	959	1.99	7.20–6.02	15.1	36.3–34.9	32.6 (28.7)
SNU-100′-Ca	$[Zn_3(TCPT)_2(HCOO)][Ca(H_2O)_n]_{0.427}[NH_2(CH_3)_2]_{0.146}$	0.142	935	1.88	8.10–6.65	15.1	37.4–36.4	40.4 (33.6)
SNU-100′-Co	$[Zn_3(TCPT)_2(HCOO)][Co(H_2O)_n]_{0.477}[NH_2(CH_3)_2]_{0.046}$	0.159	1000	2.16	7.59–7.20	16.8	36.0–34.6	31.0 (27.0)
SNU-100′-Ni	$[Zn_3(TCPT)_2(HCOO)][Ni(H_2O)_n]_{0.445}[NH_2(CH_3)_2]_{0.110}$	0.148	982	1.98	7.01–5.56	16.6	34.5–33.3	37.4 (29.6)
Mg-MOF-74[16]	$Mg_2(dobdc)$	—	1495	—	—	26.0	47	44
HKUST-1[17]	$Cu_3(BTC)_2$	—	1400	—	—	19.8	35	101
Cu-BTTri-en[5]	$H_3[(Cu_4Cl)_3(BTTri)_8(en)_{3.75}]$	—	345	—	—	5.5	90	44
Cu-BTTri-mmen[6]	$H_3[(Cu_4Cl)_3(BTTri)_8(mmen)_{12}]$	—	871	—	—	15.4	96	165
MOF-177[2a,4d]	$Zn_4O(BTB)_2$	—	4508	—	—	3.4	—	4

[a] The number of the coordinated water molecules (n) is 4–6, as estimated by ICP-AES, EA data, and theoretical calculation. [b] Measured at 77 K and 1 atm. [c] Obtained at 298 K and 1 atm. [d] Selectivities were calculated from the ratios of Henry constants for CO_2 and N_2 adsorption isotherms at 298 K and the values in parenthesis are selectivities estimated by using the molar ratio at 298 K of the CO_2 uptake at 0.15 atm and the N_2 uptake at 0.85 atm.

lower CO_2 storage capacities, and the measured PXRD pattern reveals the collapse of the framework (Fig. S35†). This means that the coordinated water molecules could not be partially removed by heating the sample up to 350 °C under vacuum.

The Q_{st} values of CH_4 adsorption were calculated by applying Langmuir–Freundlich parameters at 231, 273, and 298 K (Fig. S41–S46 and Table S9†) to the Clausius–Clapeyron equation because the Langmuir–Freundlich equation afforded a better fit to CH_4 adsorption data than the dual-site Langmuir equation (Fig. S47†). The low coverage Q_{st} values of CH_4 adsorption are also increased by the impregnated metal ions, but the enhancement (by 4.26–0.16 kJ mol^{-1}) is much smaller (Fig. S40†) than those (by 8.1–5.3 kJ mol^{-1}) for the CO_2 adsorption. Due to the significantly greater quadrupole moment and polarizability of CO_2, the interaction of CO_2 molecules with the anionic framework and extra-framework metal ions must be much stronger than that of CH_4 molecules.

The selectivities of CO_2 adsorption over N_2 for the series of **SNU-100′-M**, estimated from the ratios of Henry constants derived from the Langmuir equation (Fig. S48–S52 and Table S10†), are also significantly increased to 37.8, 32.6, 40.4, 31.0, and 37.4 for **SNU-100′-Li**, **SNU-100′-Mg**, **SNU-100′-Ca**, **SNU-100′-Co**, and **SNU-100′-Ni**, respectively, compared to 25.5 of **SNU-100′**. The enhanced selectivity of CO_2 over N_2 must be attributed to the increased interaction of CO_2 molecules with impregnated metal ions in the channels. It should be noted here that the selectivity calculations may have a large error since a single-site Langmuir equation does not fit well the Henry region of these relatively steep isotherms.

The selective and reversible capture of CO_2 at 298 K in **SNU-100′-M** as well as in **SNU-100′** was verified by the gas cycling experiment using a gas stream of 15% (v/v) CO_2 in N_2, which approximately mimics flue gas, followed by a pure N_2 gas stream (Fig. S53†). Reversible changes of 2.1 wt% in **SNU-100′-M** and 2.0 wt% in **SNU-100′** were observed over the cycles, and the material was regenerated by the N_2 gas flow.

To test the cyclability of CO_2 adsorption in **SNU-100′-Ca**, which exhibited the highest zero-coverage Q_{st} (37.4 kJ mol^{-1}) of CO_2 adsorption among the present samples, the CO_2 gas sorption isotherms were measured for ten cycles at 298 K and 1 atm on an automated micropore gas analyzer (Fig. 3). The results showed no apparent decrease in capacity over ten cycles and revealed the complete regeneration of the material just by evacuation without applying heat.

The plot of the BET surface area *versus* equivalent cation sites in **SNU-100′-M**, independent of the type of metal ions (Fig. S54†), indicates that the degree of metal ion impregnation obviously affects the surface area of the MOF, which in turn

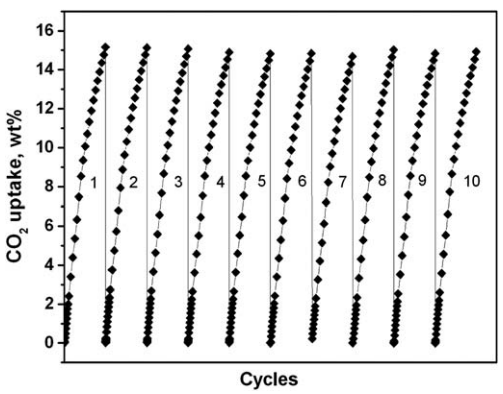

Fig. 3 Ten cycles of CO_2 uptake of **SNU-100′-Ca** at 298 K and 1 atm without the reactivation process between the cycles.

affects gas sorption properties (Fig. S55†). In this respect, we may assume that the type of metal ions has a rather minor effect (<20% change) on the CO_2 sorption properties because the sizes of metal aqua complexes are not so different.

During the introduction of metal ions, the quality of the single-crystal became unsuitable for single-crystal X-ray diffraction analysis, and thus the precise position of the incorporated metal ions in the pores could not be determined. Therefore, we conducted a "locate simulation" by using a sorption module of Materials Studio to determine the location sites of the extra-framework cations (see Experimental Section in the ESI†).[21] The results indicate that $[NH_2(CH_3)_2]^+$ cations in **SNU-100** locate near the center of the 1D channels, similarly to its single crystal X-ray structure (Fig. S28†). The metal ions coordinated with water molecules also locate near the centre of the 1D channels (Fig. S56–S62†), although bare metal ion should reside beside the benzene rings of the TCPT ligand. The divalent cations occupy half sites of the monovalent cations and they keep the distance of 14 Å from each other within the channel, the same length as the *c*-axis in a unit cell.

Theoretical accessible surface areas and total free volumes were estimated for **SNU-100′** and the series of **SNU-100′-M**, using the Atoms Volume and Surfaces calculation module of Materials Studio.[21] The simulated surface area (841 $m^2\ g^{-1}$) for **SNU-100′** is comparable to the BET surface area (814 $m^2\ g^{-1}$) derived from the measured N_2 sorption isotherm at 77 K (Table 2). The simulated surface areas of the **SNU-100′-M** series were estimated with the assumption that 100% $[NH_2(CH_3)_2]^+$ cations were exchanged with metal ions. The comparison of the simulated surface areas with the experimental values suggests that the number of coordinated water molecules at the impregnated metal ion must be four. When it was assumed that six water molecules were coordinated at the metal ion, much smaller simulated surface areas resulted than the experimental values. In addition, the fact that the activated sample of **SNU-100′-Co** showed a purple color, characteristic of the four coordinated Co^{2+} ion, which immediately changed to pale pink upon exposure to air, also supports that the number of water molecules coordinated at the metal ions is four.

We also performed Grand Canonical Monte Carlo (GCMC) calculations to estimate the Q_{st} values of CO_2 and CH_4 adsorptions for each simulated **SNU-100′-M** (Table 2), by using adsorption isotherm simulations in a Sorption module of Materials Studio (see also Experimental Section in the ESI†). The calculations were performed with the assumption that 100% $[NH_2(CH_3)_2]^+$ cations were exchanged with $M(H_2O)_4^{n+}$ ions. To elucidate the effects of electrostatic interaction on Q_{st}, additional simulations were conducted by eliminating the contribution of electrostatic interaction. The simulated Q_{st} values (26.7–25.3 kJ mol^{-1}) of CO_2 adsorption in **SNU-100′**, considering only the dispersion interaction, are comparable to those (29.3–27.7 kJ mol^{-1}) derived from the measured CO_2 adsorption isotherms. The simulated Q_{st} values for **SNU-100′-M** are remarkably increased when the electrostatic model was applied. The results clearly indicate that the highly enhanced Q_{st} values for **SNU-100′-M** must be attributed to the electrostatic interactions of CO_2 with the extra-framework metal ions as well as the interaction of CO_2 with H_2O molecules bound to the solvated extra-framework metal ions. One might assume that the enhanced interaction would be a result of the generation of narrower pockets within the pores, but this does not seem to be happening in the present case as evidenced by increased porosity on metal ion impregnation. Among various metal ions, the Ca^{2+} ion must be the best for increasing Q_{st} of the CO_2 adsorption, as seen in Table 1 and Table 2. For the CH_4 adsorption, Q_{st} values simulated by using the electrostatic model are very similar to the experimental data but they are higher just by *ca* 8–10 kJ mol^{-1} than those simulated with the non-electrostatic model. The results demonstrate that CO_2 has a much stronger tendency to have electrostatic interactions than CH_4 due to its higher polarizability and quadrupole moment.

Conclusions

Our experimental and theoretical studies clearly demonstrate that the impregnation of various metal ions such as Li^+, Mg^{2+}, Ca^{2+}, Co^{2+}, and Ni^{2+}, which are coordinated with water molecules, in the pores of an anionic MOF, $[Zn_3(TCPT)_2(HCOO)][NH_2(CH_3)_2]$ (**SNU-100′**), significantly enhances isosteric heat, selectivity, and uptake capacity of the CO_2 adsorption in the MOF at room temperature, while it affects rather slightly on H_2 and CH_4 adsorptions. The frameworks with impregnated metal ions, the **SNU-100′-M** series, reversibly adsorb and desorb CO_2 at 298 K. Due to the electrostatic interactions between CO_2 and the impregnated extra-framework metal ions, the isosteric heats of CO_2 adsorption in the **SNU-100′-M** series are increased

Table 2 Theoretical accessible free volumes, surface areas, and Q_{st} values of the CO_2 and CH_4 adsorption in the **SNU-100′-M** series[a]

			Q_{st} of CO_2/kJ mol^{-1}		Q_{st} of CH_4/kJ mol^{-1}	
Compound	Free volume[b]	Surface area[b] ($m^2\ g^{-1}$)	Non-electrostatic	Electrostatic	Non-electrostatic	Electrostatic
SNU-100′	0.188	842	26.7–25.3	55.6–49.9	19.9–19.4	29.8–27.4
SNU-100′-Li	0.153 (0.146)	736 (649)	25.7–25.0	76.4–66.8	20.6–19.9	28.1–27.1
SNU-100′-Mg	0.283 (0.252)	972 (876)	25.8–25.0	80.8–70.2	19.9–19.5	28.8–23.9
SNU-100′-Ca	0.270 (0.230)	939 (846)	24.8–25.6	85.4–72.6	19.9–19.3	28.8–26.8
SNU-100′-Co	0.253 (0.238)	912 (858)	25.2–24.4	68.3–52.4	20.3–19.8	27.9–26.2
SNU-100′-Ni	0.243 (0.230)	1000 (869)	25.3–24.5	72.4–66.4	20.3–19.9	28.6–26.2

[a] Calculated by the assumption that 100% $[NH_2(CH_3)_2]^+$ cations in **SNU-100′** are exchanged with metal ions. [b] Calculated for the tetraaqua metal ion complexes. The values in the parentheses are the values calculated for the hexaaqua complexes.

to 37.4–34.5 kJ mol^{-1}, and the effective adsorption selectivities of CO_2 over N_2 at room temperature are increased to 40.4–31.0, compared with 29.3 kJ mol^{-1} and 25.5 of the parent MOF (**SNU-100′**). Among various metal ions, the Ca^{2+} ion seems to be the best for increasing the isosteric heat of CO_2 adsorption. The present MOFs with impregnated metal ions must be good candidates as the materials for post-combustion CO_2 capture from industrial flue gas.

Acknowledgements

This work was supported by a National Research Foundation of Korea (NRF) grant funded by the Korean Government (MEST) (no. 2011-0031432 and no. 2012-0000651). The authors acknowledge the Pohang Accelerator Laboratory (PAL) for the use of the synchrotron beamline.

Notes and references

1 (*a*) M. P. Suh, H. J. Park, T. K. Prasad and D.-W. Lim, *Chem. Rev.*, 2012, **112**, 782; (*b*) J. Sculley, D. Yuan and H.-C. Zhou, *Energy Environ. Sci.*, 2011, **4**, 2721; (*c*) R. B. Getman, Y.-S. Bae, C. E. Wilmer and R. Q. Snurr, *Chem. Rev.*, 2012, **112**, 703.

2 (*a*) K. Sumida, D. L. Rogow, J. A. Mason, T. M. McDonald, E. D. Bloch, Z. R. Herm, T.-H. Bae and J. R. Long, *Chem. Rev.*, 2012, **112**, 724; (*b*) J.-R. Li, Y. Ma, M. C. McCarthy, J. Sculley, J. Yu, H.-K. Jeong, P. B. Balbuena and H.-C. Zhou, *Coord. Chem. Rev.*, 2011, **255**, 1791; (*c*) H. J. Park, Y. E. Cheon and M. P. Suh, *Chem.–Eur. J.*, 2010, **16**, 11662; (*d*) T. K. Kim and M. P. Suh, *Chem. Commun.*, 2011, **47**, 4258.

3 (*a*) E. D. Bloch, L. M. Murray, W. L. Queen, S. Chavan, S. N. Maximoff, J. P. Bigi, R. Krishna, V. K. Peterson, F. Grandjean, G. J. Long, B. Smit, S. Bordiga, C. M. Brown and J. R. Long, *J. Am. Chem. Soc.*, 2011, **133**, 14814; (*b*) L. J. Murray, M. Dincă, J. Yano, S. Chavan, S. Bordiga, C. M. Brown and J. R. Long, *J. Am. Chem. Soc.*, 2010, **132**, 7856; (*c*) Y. E. Cheon, J. Park and M. P. Suh, *Chem. Commun.*, 2009, 5436.

4 (*a*) H. Furukawa, N. Ko, Y. B. Go, N. Aratani, S. B. Choi, E. Choi, A. Ö. Yazaydın, R. Q. Snurr, M. O'Keeffe, J. Kim and O. M. Yaghi, *Science*, 2010, **329**, 424; (*b*) O. K. Farha, A. Ö. Yazaydın, I. Eryazici, C. D. Malliakas, B. G. Hauser, M. G. Kanatzidis, S. T. Nguyen, R. Q. Snurr and J. T. Hupp, *Nat. Chem.*, 2010, **2**, 944; (*c*) H. J. Park, D.-W. Lim, W. S. Yang, T.-R. Oh and M. P. Suh, *Chem.–Eur. J.*, 2011, **17**, 7251; (*d*) A. R. Millward and O. M. Yaghi, *J. Am. Chem. Soc.*, 2005, **127**, 17998.

5 A. Demessence, D. M. D'Alessandro, M. L. Foo and J. R. Long, *J. Am. Chem. Soc.*, 2009, **131**, 8784.

6 T. M. McDonald, D. M. D'Alessandro, R. Krishna and J. R. Long, *Chem. Sci.*, 2011, **2**, 2022.

7 D. Sun, Y. Ke, D. J. Collins, G. A. Lorigan and H.-C. Zhou, *Inorg. Chem.*, 2007, **46**, 2725.

8 A. L. Spek, *PLATON99, A Multipurpose Crystallographic Tool*; Utrecht University: Utrecht, The Netherlands, 1999.

9 L. Czepirski and J. Jagiello, *Chem. Eng. Sci.*, 1989, **44**, 797.

10 R. Banerjee, H. Furukawa, D. Britt, C. Knobler, M. O'Keeffe and O. M. Yaghi, *J. Am. Chem. Soc.*, 2009, **131**, 3875.

11 M. G. Nijkamp, J. E. M. J. Raaymakers, A. P. van Dillen and K. P. de Jong, *Appl. Phys. A: Mater. Sci. Process.*, 2001, **72**, 619.

12 (*a*) F. Nouar, J. Eckert, J. F. Eubank, P. Forster and M. Eddaoudi, *J. Am. Chem. Soc.*, 2009, **131**, 2864; (*b*) M. Dincă and J. R. Long, *J. Am. Chem. Soc.*, 2007, **129**, 11172; (*c*) S. Yang, X. Lin, A. J. Blake, G. S. Walker, P. Hubberstey, N. R. Champness and M. Schröder, *Nat. Chem.*, 2009, **1**, 487; (*d*) G. Calleja, J. A. Botas, M. Sanchez-Sanchez and M. G. Orcajo, *Int. J. Hydrogen Energy*, 2010, **35**, 9916; (*e*) S. Yang, G. S. B. Martin, J. J. Titman, A. J. Blake, D. R. Allan, N. R. Champness and M. Schröder, *Inorg. Chem.*, 2011, **50**, 9374.

13 (*a*) Y. G. Lee, H. R. Moon, Y. E. Cheon and M. P. Suh, *Angew. Chem., Int. Ed.*, 2008, **47**, 7741; (*b*) M. Dincă, A. Dailly, Y. Liu, C. M. Brown, D. A. Neumann and J. R. Long, *J. Am. Chem. Soc.*, 2006, **128**, 16876; (*c*) Y. E. Cheon and M. P. Suh, *Chem. Commun.*, 2009, 2296.

14 (*a*) J. L. C. Rowsell and O. M. Yaghi, *J. Am. Chem. Soc.*, 2006, **128**, 1304; (*b*) Z. Wang, K. K. Tanabe and S. M. Cohen, *Chem.–Eur. J.*, 2010, **16**, 212; (*c*) T. K. Prasad, D. H. Hong and M. P. Suh, *Chem.–Eur. J.*, 2010, **16**, 14043; (*d*) H. J. Park and M. P. Suh, *Chem. Commun.*, 2012, **48**, 3400.

15 (*a*) Y. E. Cheon and M. P. Suh, *Angew. Chem., Int. Ed.*, 2009, **48**, 2899; (*b*) L. Wang, N. R. Stuckert, H. Chen and R. T. Yang, *J. Phys. Chem. C*, 2011, **115**, 4793; (*c*) C. Zlotea, R. Campesi, F. Cuevas, E. Leroy, P. Dibandjo, C. Volkringer, T. Loiseau, G. Férey and M. Latroche, *J. Am. Chem. Soc.*, 2010, **132**, 2991; (*d*) K. L. Mulfort, O. K. Farha, C. L. Stern, A. A. Sarjeant and J. T. Hupp, *J. Am. Chem. Soc.*, 2009, **131**, 3866.

16 (*a*) C. K. Brozek and M. Dincă, *Chem. Sci.*, 2012, **3**, 2110; (*b*) Z. Zhang, L. Zhang, L. Wojtas, P. Nugent, M. Eddaoudi and M. J. Zaworotko, *J. Am. Chem. Soc.*, 2012, **134**, 924.

17 S. R. Caskey, A. G. Wong-Foy and A. J. Matzger, *J. Am. Chem. Soc.*, 2008, **130**, 10870.

18 A. Ö. Yazaydın, A. I. Benin, S. A. Faheem, P. Jakubczak, J. J. Low, R. R. Willis and R. Q. Snurr, *Chem. Mater.*, 2009, **21**, 1425.

19 (*a*) Y. F. Chen, A. Nalaparaju, M. Eddaoudi and J. W. Jiang, *Langmuir*, 2012, **28**, 3903; (*b*) P. He, H. Liu, Y. Li, Z. Lei, S. Huang, P. Wang and H. Tian, *Mol. Simul.*, 2012, **38**, 72.

20 P. L. Llewellyn, S. Bourrelly, C. Serre, A. Vimont, M. Daturi, L. Hamon, G. S. Weireld, J.-S. Chang, D.-Y. Hong, Y. K. Hwang, S. H. Jhung and G. Férey, *Langmuir*, 2008, **24**, 7245.

21 *Materials Studio v5.5*, Accelrys Inc., San Diego, CA, 2010.

